Journal of Structural Engineering & Applied Mechanics
2021 Volume 4 Issue 2 Pages 111-125
https://doi.org/10.31462/jseam.2020.04111125

www.goldenlightpublish.com

RESEARCH ARTICLE

Refined strength prediction of concrete 2D bottle-shaped struts

Abdelrazek E. Ebrahim[1], Omar M. Elmeligy[2], Salah E. El-Metwally[*3], Mashhour A. Ghoneim[4], Hamed S. Askar[3]

[1] *Badr University in Cairo (BUC), Structural Engineering Department, Cairo, Egypt*
[2] *The British University in Egypt (BUE), Civil Engineering Department, Cairo, Egypt*
[3] *Mansoura University, Structural Engineering Department, El-Mansoura, Egypt*
[4] *Cairo University, Structural Engineering Department, Giza, Egypt*

Abstract

For better strength prediction using strut-and-tie models (STM), it is essential to use reliable strength parameters of the model components; e.g., struts, ties, and nodes. Among all the elements of the STM, the strength of the bottle-shaped struts is not well quantified. The purpose of this study is to develop more accurate formulas for the calculation of the effectiveness factors for 2D bottle-shaped struts, that are unreinforced, reinforced with minimum reinforcement, and reinforced with sufficient transverse reinforcement. The nonlinear finite element analysis, with the aid of the software ABAQUS, has been utilized in this study, which has been verified against experimental tests. The study has been carried out for grades of concrete varying from 20 to 100MPa, and for bearing plate to width ratio varying from 0.1 to 0.9. The obtained formulas for the effectiveness factors of bottle-shaped struts are functions of the concrete strength, which is not the case with the ACI 318-19 provisions. These formulas have been verified against experimental tests and have been compared with the ACI 318-19 provisions. The predictions based on these formulas are more accurate than those based on the ACI 318-19 provisions. Also, the results from these formulas are always on the safe side. On the other hand, the ACI 318-19 provisions lead to unsafe results in the case of high-strength concrete and very conservative results for the case of unreinforced struts from normal-strength concrete.

Keywords

Strut-and-Tie model; Bottle-shaped struts; Effectiveness factor; Nonlinear finite element analysis; ABAQUS

Received: 09 April 2021; Accepted: 08 June 2021

ISSN: 2630-5763 (online)

1. Introduction

For better strength prediction of discontinuity regions (D-regions) using strut-and-tie models (STM), it is essential to use reliable strength parameters of the model components; e.g., the strength of struts, ties, and nodes. In an STM, struts are classified into three types; prismatic, fan-shaped, and bottle-shaped, Fig. 1. Among all the elements of the STM, the strength of the bottle-shaped struts is not well quantified.

Bottle-shaped struts are generated as the load is applied to a comparatively narrow region of the member. The compressive stress field extends out laterally as the forces pass through the member, Fig. 2.

* Corresponding author
Email: selmetwally@mans.edu.eg

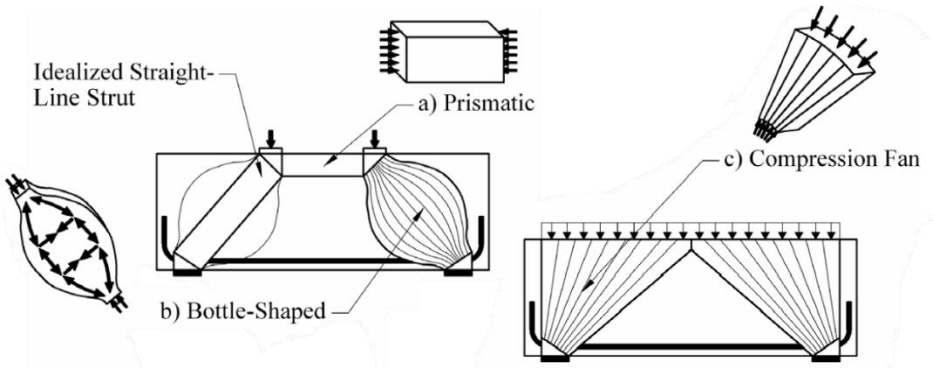

Fig. 1. Geometric shapes of struts [1].

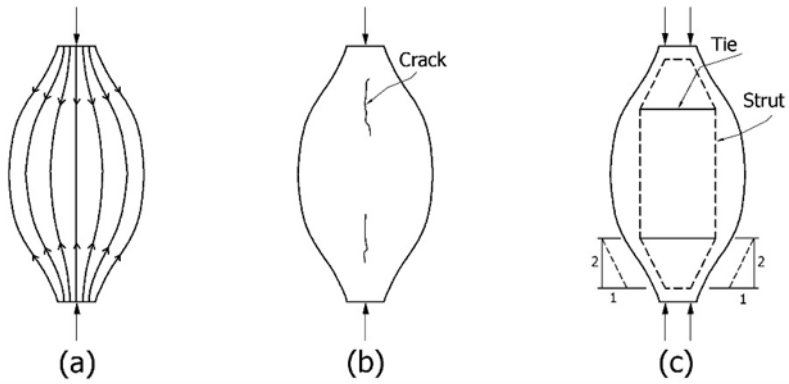

Fig. 2. Stress dispersion in bottle-shaped strut: (a) flow of forces; (b) crack pattern; and (c) strut-and-tie model.

As the compressive stress field disperses in a bottle-shaped strut, it switches direction, creating an angle with the strut's axis. In order to secure equilibrium, transverse tensile stresses must be formed in such a strut to balance the lateral portion of the inclined compressive forces, Fig. 2a. These transverse stresses normally cause the crack pattern in Fig. 2b. A bottle-shaped strut can carry load higher than the cracking load if transverse reinforcement is provided in order to carry the transverse tension caused by stress deviation. With reference to the strut-and-tie model of the bottle-shaped strut shown in Fig. 2c, the transverse tension force in the tie, T_n, is equal to half the compression in the strut, C_n, and hence the transverse reinforcement, A_s, can be calculated, Eq. (1):

$$T_n = A_s f_y \geq \frac{C_n}{2} \tag{1}$$

Many factors influence the strength of bottle-shaped struts, such as concrete strength, strain and stress conditions in the struts, brittle nature of concrete, provided reinforcement, the angle between the strut and intersecting tie, amount of confining reinforcement, and extent of the cracks [2]. The effects of these factors are lumped together into what is called the "Effectiveness Factor" which gives the strength of the strut as a percentage of the uniaxial concrete strength. So as to calculate the strength of bottle-shaped struts for design requirements, the effectiveness factor, β_s , can be assessed experimentally or using a nonlinear finite element analysis,

$$\beta_s = \frac{f_b}{0.85\, f_c'} \tag{2}$$

where f_b is the bearing stress at failure, f_c' is the concrete cylinder strength, and 0.85 is the size effect.

In design, according to the ACI 318-19 [3], the nominal compressive strength of a strut F_{ns} shall be computed as given in Eq. (3),

$$F_{ns} = f_{ce}A_{cs} \quad (3)$$

where A_{cs} is the cross-sectional area at the end of the strut, and f_{ce} is the effective concrete strength of the strut $= 0.85\beta_c\beta_s f_c'$, β_c is the strut and node confinement modification factor, Table 1, and β_s is the strut effectiveness factor, Table 2.

In this paper, new equations are developed for predicting the effectiveness factor of 2D bottle-shaped struts. In order to achieve the objectives of this study, the 3D nonlinear finite element analysis using the software ABAQUS is utilized.

2. Research significance

The ACI 318-19 [3] assumes a constant effectiveness factor of the bottle-shaped strut based on the cracking state of the strut, location, and whether or not adequate reinforcement is provided to avoid transverse tensile cracking. This effectiveness factor does not account for the concrete strength or different levels or no transverse reinforcement of the strut.

Table 1. The ACI 318-19 Strut and node confinement modification factor β_c [3]

Location	β_c	
• End of a strut connected to a node that includes a bearing surface • Node that includes a bearing surface	Lesser of	$\sqrt{A_2/A_1}$, where A_1 defines the bearing surface
		2.0
Other cases	1.0	

Table 2. The ACI 318-19 Strut coefficient β_s [3]

Strut location	Strut type	Criteria	β_s
Tension members or tension zones of members	Any	All cases	0.4
Other cases	Boundary struts	All cases	1.0
	Interior struts	Reinforcement satisfying table 3	0.75
		Located in regions satisfying the following Eq. $Vu \leq 0.42\varphi\tan\theta\lambda\lambda s\sqrt{f_c' bwd}$	0.75
		Beam-column joints	0.75
		All other cases	0.4

where V_u is the factored shear force at section, φ is the strength reduction factor, θ is the strut angle with respect to horizontal tie, λ is a modification factor to reflect the reduced mechanical properties of lightweight concrete relative to normalweight concrete of the same compressive strength, λ_s is size effect modification factor, b_w is web width, and d is the depth of the section.

Table 3. The ACI 318-19 Minimum distributed reinforcement [3]

Lateral restraint of strut	Reinforcement configuration	Minimum distributed reinforcement ratio
Not restrained	Orthogonal grid	0.0025 in each direction
	Reinforcement in one direction crossing strut at angle $\alpha 1$	$\frac{0.0025}{sin^2\,\alpha 1}$
Restrained	Distributed reinforcement not required	

It has been demonstrated that this provision is conservative for normal strength concrete and unsafe for high strength concrete. Besides, the provision does not apply for different levels of transverse reinforcement [4]. Therefore, it is essential to deeply examine the strength of bottle-shaped struts and establish simple equations for computing their effectiveness factors.

3. Research methodology

First, the reliability of the nonlinear finite element analysis, *NFEA*, using the software ABAQUS in modeling reinforced concrete D-regions is verified against experimental results from literature. Upon comparing the two sets of results, an excellent correlation between the NFEA and the tests becomes very clear, and hence the reliability of the *NFEA* is established. Afterwards, three sets of isolated bottle-shaped struts; unreinforced, reinforced with the minimum limit given by the ACI 318-19, and sufficiently reinforced to resist transverse tension caused by stress deviation, are modeled using the *NFEA*. In each set, the concrete compressive strength is varied to include both normal and high-strength concrete; in addition, different plate-to-width ratios are considered. The ultimate load is obtained for each case. From the obtained results, the effectiveness factor of each set of struts is proposed. Upon employing curve fitting and ensuring safe factors, the proposed equations are derived for the estimate of the effectiveness factor of bottle-shaped struts, β_s. Then, the proposed effectiveness factors are verified using experimental tests of D-regions and are compared with those given by the ACI 318-19.

4. 3D Nonlinear finite element analysis, *NFEA*

4.1. Element modeling

The concrete and the loading plates are modeled using the 8-node 3D hexahedral element C3D8R, with a reduced integrated continuum hourglass control option. As for the reinforcement, it is modeled using the 2- node T3D2 truss element with assigned steel material properties and cross-sectional area of the reinforcing bars [5].

4.2. Material modeling

For modeling the real behavior of concrete, there are problems encountered if either elastic damage models or elastic plastic laws are considered. According to Sümer and Aktaş [6], in elastic damage model, it is not possible to model irreversible strains, since zero stress will correspond to zero strain which overestimates the damage value, Fig. 3b. On the other hand, when using elastic plastic model, this will result in an overestimate of the strain since the unloading curve follows the initial elastic slope [6], Fig. 3c. Hence, concrete damaged plasticity (CDP) constitutive model is a good approach for combining the two previously discussed models together to model the experimental behavior of concrete [7], Fig. 3a. Therefore, concrete damaged plasticity is the model adopted in this study

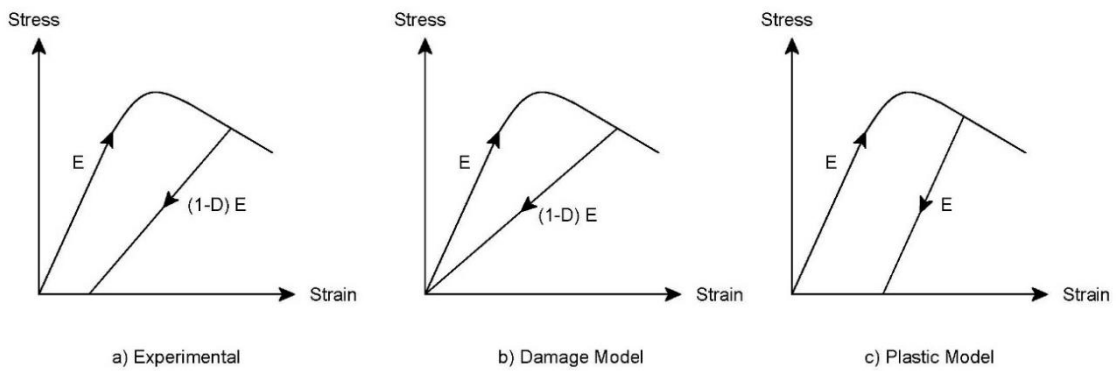

Fig. 3. Some concrete constitutive models

In concrete damaged plasticity constitutive model, the two main mechanisms for failure are compressive crushing and tensile cracking of concrete. The development of yield surface "failure surface" is controlled by equivalent compression and tension plastic strains. During failure, successive reduction in material stiffness and irreversible deformations occur; this results in strain softening in tension and low-confined and unconfined compression. In low-confined compression, large inelastic volumetric expansions happen; however, stiffness reduction and inelastic volume changes are highly reduced for highly-confined compression [8].

In the development of the constitutive model using of CDP model, different parameters are required to be defined such as; the uniaxial behavior of concrete under compression and tension, compression and tension damage parameters, plasticity parameters. The model proposed by Thorenfeldt et al. [9], Fig. 4, is adopted to simulate the concrete uniaxial behavior in compression with cylinder strength ranging between 15 to 125 MPa. This model is expressed by Eq. (4) in which, f_c' is the cylinder strength,

$$\frac{\boldsymbol{f_c}}{f_c'} = \frac{\boldsymbol{n(\epsilon_c/\varepsilon_o)}}{\boldsymbol{n-1+(\epsilon_c/\varepsilon_o)^{nk}}} \tag{4}$$

where ε_o is the strain obtained when f_c is equal to $f_c' = \frac{f_c'}{E_c}\left(\frac{n}{n-1}\right)$; n is a curve-fitting factor $= 0.8 + \frac{29 f_c'}{500}$, f_c' is in MPa; E_c is the initial tangent modulus $= 4500\sqrt{f_c'}$ MPa for normal-weight concrete; and k is a factor that controls the slopes of the ascending and the descending branches of the stress-strain curve:

- $k = 1$ for $\epsilon_c/\varepsilon_o \leq 1.0$
- $k = 0.67 + \frac{29 f_c'}{1800} \geq 1.0\ (MPa)$ for $\epsilon_c/\varepsilon_o \geq 1.0$

For the concrete uniaxial behavior in tension, the relationship between stress and strain can be assumed linear with slope E_0, until reaching the maximum stress f_t and a corresponding strain ε_{to}. After reaching the maximum stress f_t, concrete will start to crack, the post-failure behavior of cracked concrete can be modeled using the tension stiffening model proposed by Wahalathantri et al. [10], Fig. 5, which considers the interaction between reinforcement and cracked concrete.

The damage parameters d_c and d_t of compression and tension, respectively, are introduced to the model only in the descending part of the stress-strain curves according to Jankowiak and Lodygowski [11], as given by Eqs. (6) and (7).

$$d_c = 1 - \frac{f_c}{f_c'} \tag{5}$$

$$d_t = 1 - \frac{\sigma_t}{f_t} \tag{6}$$

The uniaxial stress-strain relation of concrete in compression is defined in ABAQUS in terms of inelastic strain $\tilde{\epsilon}_c^{in}$;

$$\tilde{\epsilon}_c^{in} = \epsilon_c - \tilde{\epsilon}_{oc}^{el}, \tilde{\epsilon}_{oc}^{el} = \frac{\sigma_c}{E_o} \tag{7}$$

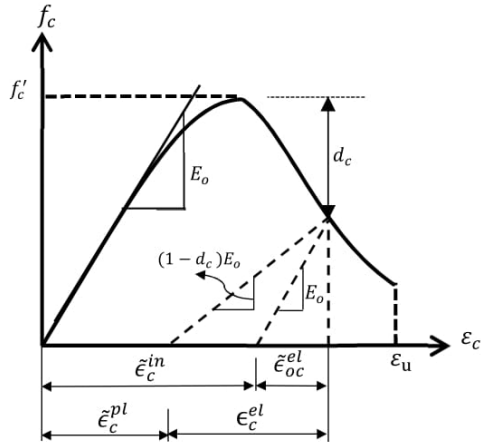

Fig. 4. Definition of concrete uniaxial behavior in compression

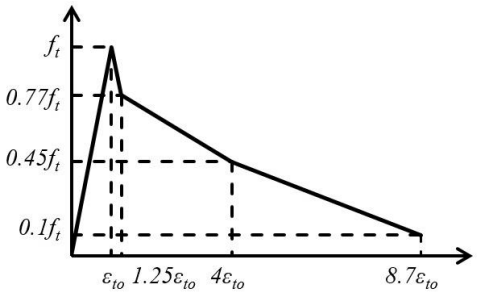

Fig. 5. Tension stiffening model

where σ_c is the corresponding compressive stress f_c and E_o is the initial elastic modulus. The inelastic strain $\tilde{\epsilon}_c^{in}$ is converted into plastic stain $\tilde{\epsilon}_c^{pl}$ using the input data for the damage parameter d_c as follows;

$$\tilde{\epsilon}_c^{pl} = \tilde{\epsilon}_c^{in} - \frac{d_c}{(1-d_c)}\frac{\sigma_c}{E_0} \quad (8)$$

Similarly, the stress-strain relation in uniaxial tension is defined in terms of a cracking strain $\tilde{\epsilon}_t^{ck}$;

$$\tilde{\epsilon}_t^{ck} = \epsilon_t - \tilde{\epsilon}_{ot}^{el}, \tilde{\epsilon}_{ot}^{el} = \frac{\sigma_t}{E_o} \quad (9)$$

where σ_t is the tensile stress. The cracking strain $\tilde{\epsilon}_t^{ck}$ is converted into plastic stain $\tilde{\epsilon}_t^{pl}$ using the input data for the damage parameter d_t

$$\tilde{\epsilon}_t^{pl} = \tilde{\epsilon}_t^{ck} - \frac{d_t}{(1-d_t)}\frac{\sigma_t}{E_0} \quad (10)$$

The main parameters for the CDP model are the dilation angel of concrete, the eccentricity, and its default value is 0.1, which means that the material's dilation angle is nearly constant over a broad range of confining pressure stress values, the ratio between the second stress invariant on the tensile meridian and the compressive meridian parameter, $0.5 < K_c \leq 1$, at the initial yield, this condition must be achieved, the ratio between the concrete biaxial compressive strength, σ_{b0}, and the concrete uniaxial compressive strength, σ_{c0}, and the viscosity parameter, μ. Many researchers investigated these parameters' effect and suggested the optimum range for these parameters. The chosen values of these parameters, Table 4, have given the best fit with the experimental results and fall in the recommended range as reported by Jankowiak and Lodygowski [11], Sümer and Aktaş [6], and SIMULIA [5].

In modeling the steel reinforcement, it is assumed to behave as an elastic perfectly-plastic material [6]. The elastic modulus of steel is taken as 200 GPa unless otherwise stated, and Poisson's ratio is assumed equal to 0.3. In this study, a perfect bond between reinforcement and concrete has been assumed. The reinforcing bar is embedded into the concrete host element; thus, all embedded element nodes have the same translational degrees of freedom as the concrete host element's nodes [5].

4.3. Analysis verification

In order to verify the numerical solutions from the *NFEA*, three examples of various D-regions that have been tested experimentally are modeled. The obtained results in terms of failure load and load-displacement relation, are given along with the measured values, in Table 5 and Fig. 6. Upon comparing the two sets of results, an excellent correlation between the *NFEA* and the tests is very clear, and hence the reliability of the *NFEA* is established.

Table 4. Plasticity parameters used in ABAQUS

Dilation angel	Eccentricity	K_c	σ_{b0}/σ_{c0}	Viscosity parameter
38°	0.1	0.667	1.12	0.00035

Table 5. ABAQUS verification results

D-Region	Specimen Number	f_c' (MPa)	Exp. Failure Load (kN)	*NFEA* Failure Load (kN)	*NFEA* Failure Load /Test Failure Load
Simple Deep Beam, Zhang and Tan [12]	3DB100b	29.3	1344	1402.89	1.04
Continuous Deep Beam, Yang et al. [13]	H6NN	65.1	2248	2294.79	1.02
Beam with Opening, Yang and Ashour [14]	6INN	50.5	1459	1468.85	1.01

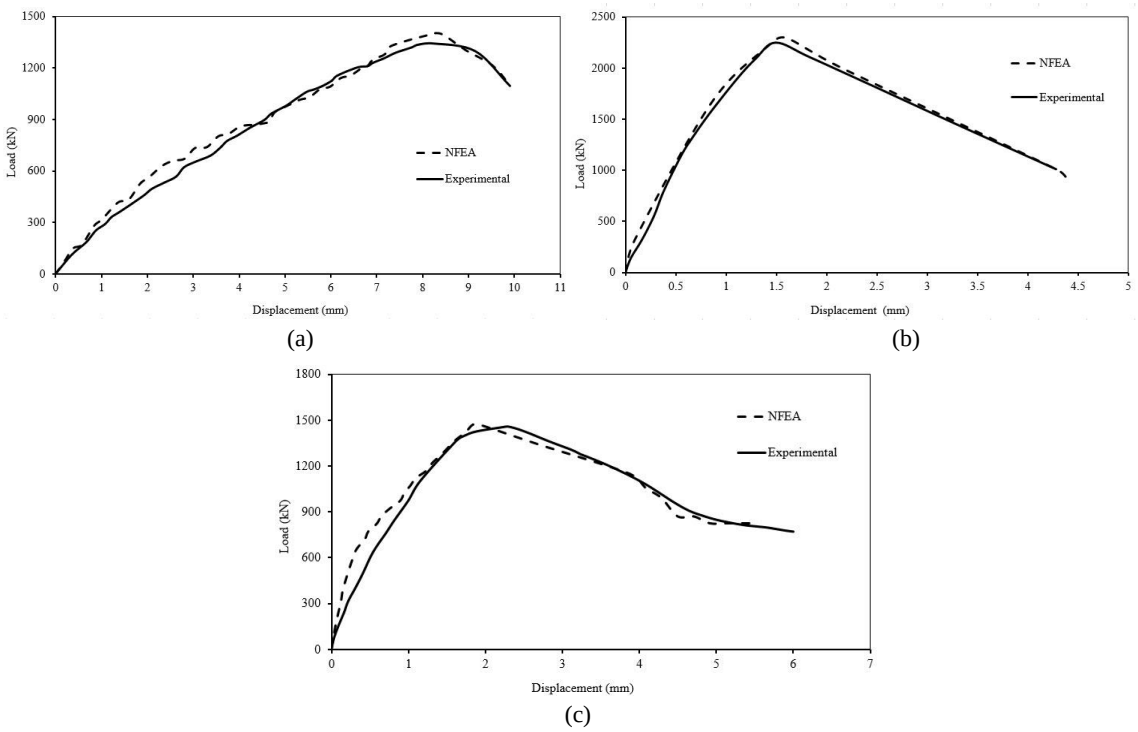

Fig. 6. Load-displacement curves of verification specimens: (a) 3DB100b; (b) H6NN; and (c) 6INN

5. Assessment of the effectiveness factor

In this research, a wide range of isolated specimens, Fig. 7, has been modeled using NFEA in order to estimate the effectiveness factor of bottle-shaped struts. The dimensions of any specimen are 600×600×80 mm. The models are classified into three types; unreinforced specimens, specimens with the minimum reinforcement ratio as defined by the ACI318-19, specimens with sufficient steel bars to resist the transverse tension force according to Eq. (1).

The concrete strength of the specimens varied from 20 to 100 MPa, with an increment of 10 MPa, in order to clarify the variation of the effectiveness factor with the concrete strength. Also, the area of the bearing plate varied by changing the plate width, a, from 0.1 to 0.9 the specimen width, b, for each grade of the concrete strength, Table 6, Fig. 7.

The ultimate load is obtained for each model using *NFEA*. For each grade of concrete, the effectiveness factors are determined for the three sets of models. Fig. 8 shows samples of the results.

6. Proposed equations for the effectiveness factor of 2d bottle-shaped struts

From the *NFEA* results of the three sets of specimens of the preceding section, it's clear that the effectiveness factor β_s depends on the concrete strength, f_c', for either set. Upon employing curve fitting and ensuring safe factors, the following equations, Eqs. (11) to (13), have been derived for the estimate of the effectiveness factor of bottle-shaped struts, β_s.

For unreinforced bottle-shaped struts,

$$\beta_s = 0.45 + 4 \times 10^{-5}(100 - f_c')^2 \quad (11)$$

For bottle-shaped struts with minimum reinforcement ratio as defined by the ACI318-19,

$$\beta_s = 0.48 + 6 \times 10^{-5}(100 - f_c')^2 \quad (12)$$

For bottle-shaped struts with sufficient reinforcement to resist the transverse tension according to Eq. (1),

$$\beta_s = 0.55 + 8 \times 10^{-5}(100 - f_c')^2 \quad (13)$$

Eqs. (11) to (13) are plotted in Figs. 9 to 11, along with the minimum values of β_s obtained from

the *NFEA*, for each grade of concrete, in order to show that the estimates given by the equations are on the safe side. The ACI 318-19 provisions are also given in the plots, and the comparison shows that these provisions are conservative for the case of unreinforced struts, especially when f_c' gets lower. For struts with minimum reinforcement, the ACI 318-19 provisions are unsafe for $f_c' > 32$ MPa, and for struts with adequate transverse reinforcement, they are unsafe for $f_c' > 50$ MPa. The three equations are plotted in Fig. 12 along with the ACI 318-19 provisions.

7. Verification of proposed effectiveness factors

In order to verify the reliability of the proposed equations for the effectiveness factors of bottle-shaped struts, several reinforced concrete D-regions, such as simple deep beams, continuous deep beams, and corbels, that have been tested experimentally, are utilized. Two sets of solutions for the collapse load of these regions based on the STM are calculated, with the ACI 318-19 provisions employed but in one set of the solutions, the proposed equations for β_s replace the ACI provisions.

7.1. Simple deep beams

Different simple deep beams have been used in the verification of the proposed equations for the effectiveness factors of bottle-shaped struts. These beams were tested by Zhang and Tan [12], Smith and Vantsiotis [15], Rogowsky et al. [16], Abdul-Razzaq and Jebur [17], Li [18], and Li [19]. The tests were carried out under single-point load and two-point loads. The details of the beams are given in table 7, and the STMs used in the calculation procedure are illustrated in Fig. 13 [20].

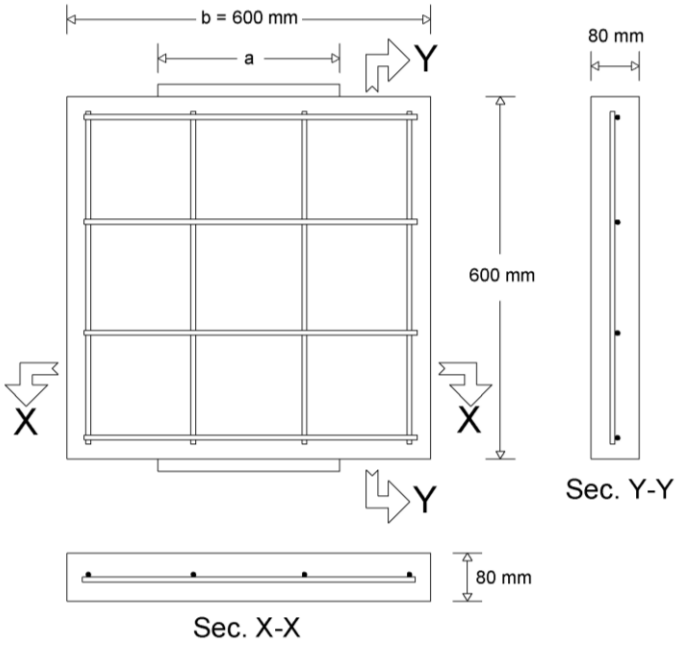

Fig. 7. Dimensions of the specimen used in the analysis

Table 6. Different widths of used plates for each grade of concrete strength

Specimen	a (mm)	Specimen	a (mm)	Specimen	a (mm)
a/b = 0.1	60	a/b = 0.4	240	a/b = 0.7	420
a/b = 0.2	120	a/b = 0.5	300	a/b = 0.8	480
a/b = 0.3	180	a/b = 0.6	360	a/b = 0.9	540

where b = 600mm is the width of the specimen

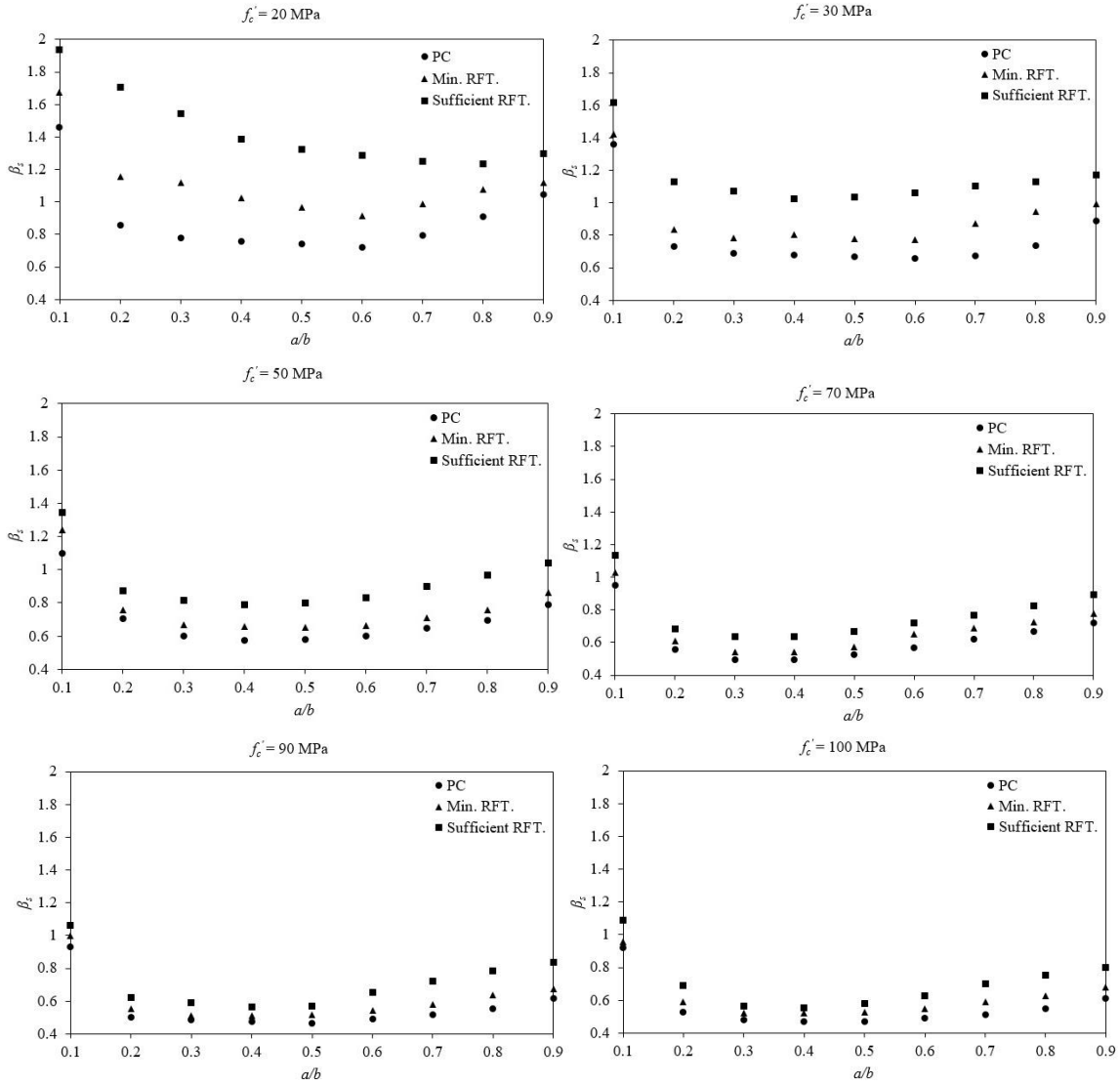

Fig. 8. Effectiveness factor versus a/b ratio for selected concrete grades.

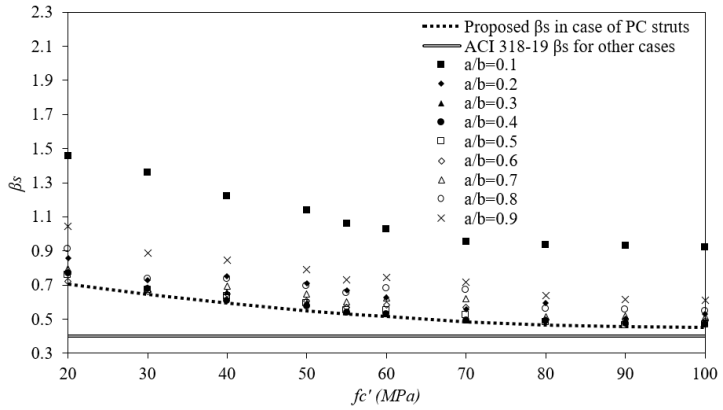

Fig. 9. Proposed effectiveness factor for unreinforced specimens

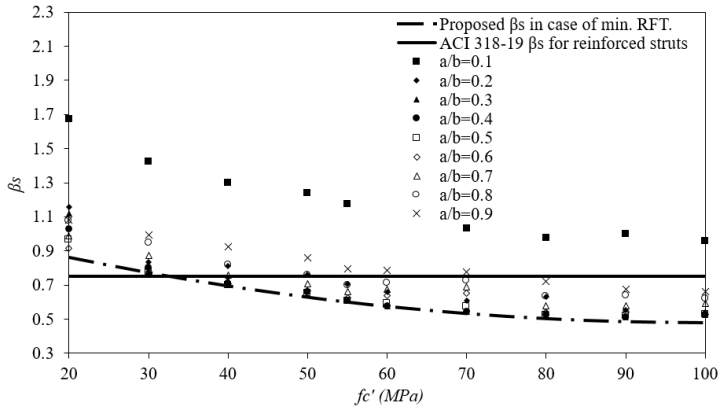

Fig. 10. Proposed effectiveness factor for specimens with minimum reinforcement

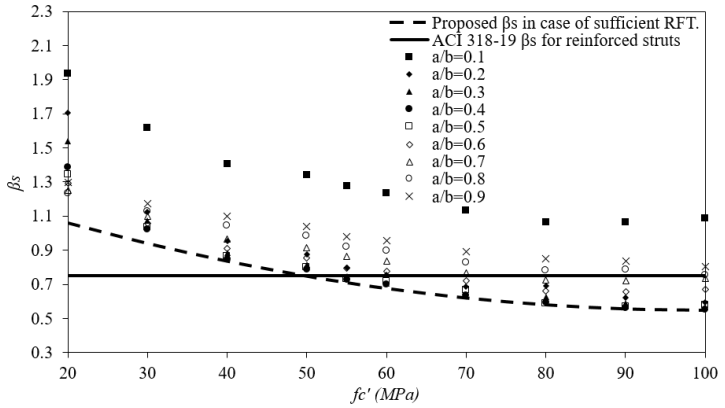

Fig. 11. Proposed effectiveness factor for specimens with adequate transverse reinforcement

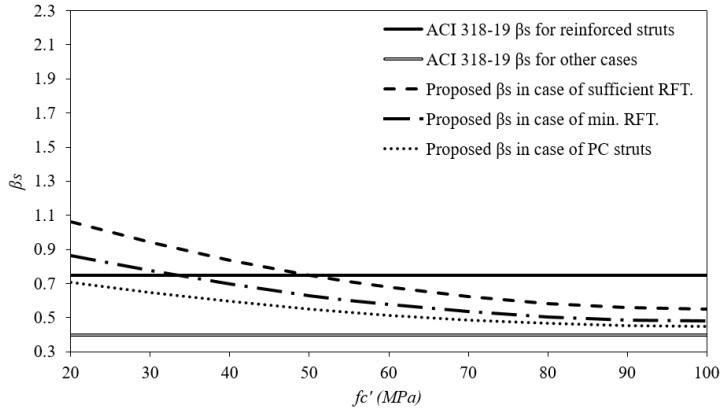

Fig. 12. Proposed effectiveness factors compared with the ACI 318-19

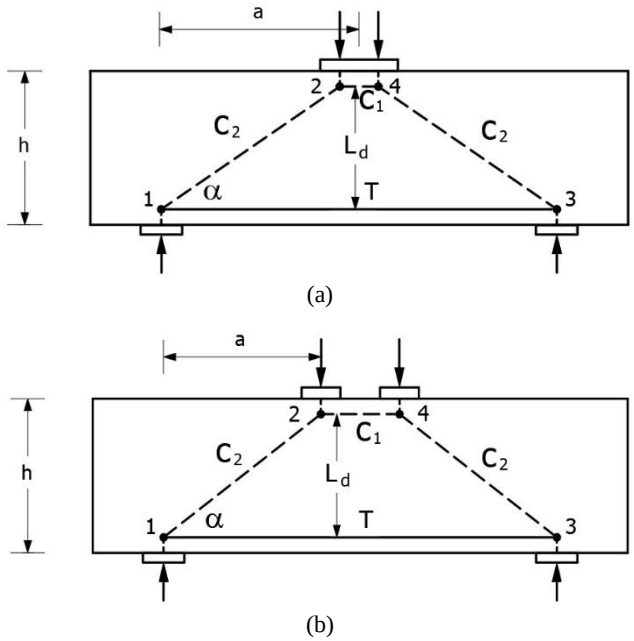

Fig. 13. STM of the simple deep beam example [20]: (a) single-point load; and (b) two-point loads

7.2. Continuous deep beams

The continuous deep beams tested by Yang et al. [13], Ashour [21], and Ashour [22] are used in this verification procedure. The details of the beams are given in Table 8, and the STMs used in the calculation procedure are illustrated in Figs. 14 and 15 [20].

7.3. Corbels

The corbels tested by Yong and Balaguru [23], Zeller [24], Cook and Mitchell [25], and Abdul-Razzaq and Dawood [26] are also used in this verification. The details of the corbels are given in Table 9, and the STM used in the calculation procedure is illustrated in Fig. 16.

7.4. Verfication results

The results of the collapse loads of all the specimens used in the verification procedure are given in tables 7 to 9. The results reveal that the proposed equations always lead to safe solutions, whereas the ACI 318-19 provisions lead to unsafe solutions in case of high strength concrete. In addition, the results from the proposed equations are more accurate in comparison with the ACI 318-19 provisions when compared with tests.

8. Summary and conclusions

The purpose of this study is to develop more accurate formulas for the calculation of the effectiveness factors for 2D bottle-shaped struts, that are unreinforced struts, reinforced with minimum reinforcement, and reinforced with sufficient transverse reinforcement. The NFEA has been utilized to achieve this study, which has been verified against experimental tests, and the analysis has shown very accurate predictions. The study has been carried out for grades of concrete varying from 20 to 100MPa, and for bearing plate to width ratio varying from 0.1 to 0.9.

The obtained formulas have been verified against experimental tests, and have been compared with the ACI 318-19 provisions. The predictions based on the developed formulas are more accurate than those obtained with the ACI 318-19 provisions. Also, the results from these formulas are always on the safe side. On the other hand, the ACI 318-19 provisions lead to unsafe results in the case of high-strength concrete and very conservative results for the case of unreinforced struts with normal-strength concrete.

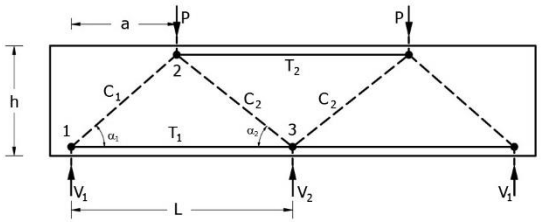

Fig. 14. Simplified STM for a continuous deep beam [20]

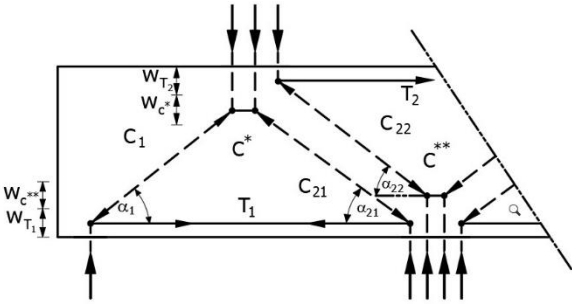

Fig. 15. Refined STM for a continuous deep beam [20]

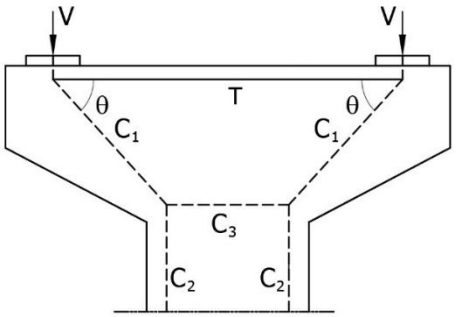

Fig. 16. Strut-and-Tie model for corbel [20].

Table 7. Verification examples of simple deep beams specimens

Investigator	Specimen	f_c'	Experimental load P_{EXP} (kN)	ACI 318-19		Proposed	
				P_{ACI} (kN)	P_{ACI}/P_{EXP} %	P_{Prop} (kN)	P_{Prop}/P_{EXP} %
Zhang and Tan [12]	1DB35bw	25.9	199	142.19	71.45	147.94	74.34
	1DB50bw	27.4	373	307.23	82.37	321.40	86.17
	1DB70bw	28.3	854	607.58	71.15	646.60	75.71
	1DB100bw	28.7	1550	1294.84	83.54	1346.60	86.88
	2DB35	27.4	170	80.64	47.44	133.22	78.36
	2DB50	32.4	271	137.57	50.76	217.62	80.30
	2DB70	24.8	311	142.44	45.80	240.80	77.43
	2DB100	30.6	483	256.99	53.21	412.89	85.48
	3DB35b	27.4	170	80.64	47.44	133.22	78.36
	3DB50b	28.3	334	169.78	50.83	278.28	83.32
	3DB70b	28.7	721	329.19	45.66	537.69	74.58
	3DB100b	29.3	1344	690.58	51.38	1127.97	83.93
Smith and Vantsiotis [15]	0A0-48	20.9	272.2	126.71	46.6	221.83	81.5
Rogowsky et al. [16]	Beam1/1.5	42.4	606	524.56	86.56	589.75	97.32
Abdul-Razzaq and Jebur [17]	B.1F	34.4	355	307.02	86.48	307.02	86.48
	B.2F	35	562	487.78	86.79	499.8	88.93
	B.W	34.1	547.8	424.56	77.5	452.86	82.67
Li [18]	B-1S	38.6	857.2	701.7448	81.86	701.74	81.86
	B-2N	38.6	1470.8	1136.38	77.26	1166.84	79.33
	B-2S	38.6	1602	1166.838	72.84	1166.84	72.84
Li [19]	B-3N	38.6	2020	1659.1	82.13	1728.16	85.55
	B-3S	38.6	2580	1728.157	66.98	1728.16	66.98
	B-4N	38.6	3247.2	2594.37	79.90	2797.77	86.16
	B-4S	38.6	4568	2817.049	61.67	2818.72	61.71

Table 8. Verification examples of cont. Deep beam specimens

Investigator	Specimen	f_c'	Experimental Load $P_{EXP.}$ (kN)	ACI 318-19		Proposed	
				P_{ACI} (kN)	P_{ACI}/P_{EXP} %	P_{Prop} (kN)	P_{Prop}/P_{EXP} %
Yang et al. [13]	L5NN	32.4	1635	521.46	31.89	824.94	50.46
	L5NS	32.4	1710	977.74	57.18	1043.77	61.04
	L5NT	32.4	1789	977.74	54.65	1043.77	58.34
	L5SN	32.4	1887	977.74	51.81	1043.77	55.31
	L5SS	32.4	2117	977.74	46.19	1043.77	49.30
	L5TN	32.4	2317	977.74	42.20	1043.77	45.05
	L10NN	32.1	880	458.72	52.13	727.55	82.68
	L10NS	32.1	1153	860.10	74.60	917.44	79.57
	L10NT	32.1	1521	860.10	55.81	917.44	59.54
	L10SS	32.1	1177	860.10	73.08	917.44	77.95
	L10TN	32.1	935	860.10	91.99	917.44	98.12
	H10NS	68.2	1443	1827.37	126.64	1305.86	90.50
	H10SN	68.2	1309	1827.37	139.60	1305.86	99.76
	H10SS	68.2	1575	1827.37	116.02	1537.18	97.60
Ashour [21]	CDB1	30.6	1100	888.42	80.77	903.21	82.11
Ashour [22]	CDB1	30	1100	570.85	51.90	570.85	51.90
	CDB2	33.1	950	629.84	66.30	629.84	66.30
	CDB3	22	570	418.62	73.44	418.62	73.44
	CDB4	28	885	532.79	60.20	532.79	60.20
	CDB5	28.7	820	546.67	66.67	546.67	66.67
	CDB6	22.5	495	330.16	66.70	353.22	71.36
	CDB7	26.7	445	392.96	88.31	419.16	94.19
	CDB8	23.6	385	367.58	95.48	380.10	98.73

Table 9. Verification examples of corbels specimens

Investigator	Specimen	f_c'	Experimental load P_{EXP} (kN)	ACI 318-19		Proposed	
				P_{ACI} (kN)	P_{ACI}/P_{EXP} %	P_{Prop} (kN)	P_{Prop}/P_{EXP} %
Yong and Balaguru [23]	B1	49.8	778.2	347.46	44.65	348.62	44.80
	B2	48.6	667.2	346.74	51.97	347.37	52.06
	D1	39.2	700.6	476.95	68.08	490.92	70.07
Zeller [24]	C	26.3	1425	1222.17	85.77	1303.65	91.48
Cook and Mitchell [25]	C	40.4	502	467.13	93.05	480.76	95.77
Abdul-Razzaq and Dawood [26]	C0.5	33.1	566	440.07	77.75	465.21	82.19
	C1	33.6	450	327.89	72.86	338.94	75.32
	C1.5	33.8	362	229.39	63.37	235.62	65.09

Ethics Committee Permission

The authors acquired ethics committee permission for surveys implemented in this paper from the Science and Engineering Fields Human Subjects Ethics Committee of Boğaziçi University (No. 84391427-050.01.04-E.17947).

Declaration of conflicting interests

The author(s) declared no potential conflicts of interest with respect to the research, authorship, and/or publication of this article.

References

[1] Bahen NP. Strut-and-tie modeling for disturbed regions in structural concrete members with emphasis on deep beams. MSc Thesis. University of Nevada, 2007.

[2] Foster SJ, Malik AR (2002) Evaluation of efficiency factor models used in strut-and-tie modeling of nonflexural member. Journal of Structural Engineering 128(5): 569-577.

[3] ACI Committee 318. Building code requirements for structural concrete (ACI 318-19) and commentary. American Concrete Institute, Farmington Hills, Michigan, 2019.

[4] Quintero-Febres CG, Parra-Montesinos G, and Wight JK (2006) Strength of struts in deep concrete members designed using strut-and-tie method. ACI Structural Journal 103(4): 577-586.

[5] SIMULIA. Abaqus/CAE User's Manual, Providence, RI, USA, 2012.

[6] Sümer Y, Aktaş M (2015) Defining parameters for concrete damage plasticity model. Challenge Journal of Structural Mechanics 1(3): 149-155.

[7] Jason L, Pijaudier-Cabot G, Huerta A, Ghavamiano S. Damage and plasticity for concrete behavior. European Congress on Com-putational Methods in Applied Sciences and Engineering, 24-28 July 2004, Jyväskylä, Finland.

[8] Grassl P, Jirásek M (2006) Damage-plastic model for concrete failure. International journal of solids and structures 43(22-23): 7166-7196.

[9] Thorenfeldt E, Tomaszewicz A, Jensen JJ. Mechanical Properties of High Strength Concrete and Application to Design. Proceedings of the Symposium: Utilization of High-Strength Concrete, Stavanger, Norway, Tapir, Trondheim, 1987.

[10] Wahalathantri BL, Thambiratnam D, Chan T, Fawzia S. A material model for flexural crack simulation in reinforced concrete elements using ABAQUS. Proceedings of the first international conference on engineering, designing and developing the built environment for sustainable wellbeing, 2011, Queensland University of Technology, Australia.

[11] Jankowiak T, Lodygowski T (2005) Identification of parameters of concrete damage plasticity constitutive model. Foundations of civil and environmental engineering 6(1): 53-69.

[12] Zhang N, Tan KH (2007) Size effect in RC deep beams: Experimental investigation and STM verification. Engineering Structures 29(12): 3241-3254.

[13] Yang KH, Chung HS, Ashour AF (2007) Influence of shear reinforcement on reinforced concrete continuous deep beams. ACI Structural Journal 104: 420-429.

[14] Yang KH, Ashour AF (2008) Effectiveness of Web Reinforcement around Openings in Continuous Concrete Deep Beams. ACI Structural journal 105: 414-424.

[15] Smith K, Vantsiotis A (1982) Shear strength of deep beams. ACI Journal Proceedings 79(3): 201-213.

[16] Rogowsky DM, MacGregor JG, Ong SY (1986) Tests of Reinforced Concrete Deep Beams. ACI Journal Proceedings 83(4): 614-623.

[17] Abdul-Razzaq KS, Jebur SF (2017) Experimental verification of strut and tie method for reinforced concrete deep beams under various types of loadings. Journal of Engineering and Sustainable Development 21(6): 39-55.

[18] Li D. Behaviour and Modeling of Deep Beams with High Shear Span-to-Depth Ratios. MSc thesis. McGill University, 2003.

[19] Li ZY. Behaviour and modeling of deep beams with low shear span-to-depth ratios. MSc thesis. McGill University, 2003.

[20] El-Metwally SE, Chen WF. Structural Concrete: Strut-and-Tie Models for Unified Design. CRC Press, Boca Raton, 2017.

[21] Ashour AF (1997) Tests of reinforced concrete continuous deep beams. ACI Structural Journal 94(1): 3-12.

[22] Ashour AF (1996) Experimental behaviour of reinforced concrete continuous deep beams. WIT Transactions on The Built Environment 17: 267-277.

[23] Yong YK, Balaguru P (1994) Behavior of Reinforced High-Strength-Concrete Corbels. Journal of Structural Engineering 120(4):1182-1201.

[24] Zeller W. Bruchversuche an Stahlbetonkonsolen bei Veraenderung des Bewehrungsgrades (Failure Tests on Reinforced Concrete Corbels with Different Reinforcement). Abschlussbericht zum Forschungsvorhaben, Institut f. Massivbau und Baustofftechnologie, Universitaet Karlsruhe, 1983.

[25] Cook WD, Mitchell D (1988) Studies of disturbed regions near discontinuities in reinforced concrete members. Structural Journal 85(2): 206-216.

[26] Abdul-Razzaq KS, Dawood AA (2020) Corbel strut and tie modeling – Experimental verification. Structures 26: 327-339.